Anal Bioanal Chem (2015) 407:4629–4638
DOI 10.1007/s00216-015-8659-5

RESEARCH PAPER

Structural characterization of multiple pyoverdines secreted by two *Pseudomonas* strains using liquid chromatography-high resolution tandem mass spectrometry with varying dissociation energies

Hua Wei[1] · **Ludmilla Aristilde**[1]

Received: 4 February 2015 / Revised: 23 March 2015 / Accepted: 24 March 2015 / Published online: 21 April 2015

Abstract High-affinity iron (Fe)-scavenging molecules, or siderophores, are secreted by microorganisms to acquire and compete for Fe. Pyoverdine (PVD), the primary siderophore produced by *Pseudomonas*, consists of a dihydroxyquinoline-type chromophore, a peptide chain of variable length and conformation, and a side chain composed of a dicarboxylic acid or its monoamide derivative. Elucidation of the PVD structures secreted by different *Pseudomonas* strains is an important step toward understanding their Fe-transport strategies. In this study, we characterized multiple PVDs secreted by *Pseudomonas putida* KT2440 and *Pseudomonas fluorescens* RA12 using ultra-high performance liquid chromatography coupled with high-resolution quadrupole-orbitrap tandem mass spectrometry. To avoid purification steps prior to characterizing the bacterial supernatants, PVD candidates were identified by extracting fragments of the dihydroxyquinoline component from the chromatographic peaks. Varying collisional dissociation energies were subsequently applied to achieve, with high mass accuracy, a broad coverage of fragments of the entire PVD. Our approach allowed us to discriminate between three different PVD structures in the secretion of each strain. The three PVDs of *P. putida* possess the same peptide chain of seven amino acids, Asp-Orn-OHAsp-Dab-Gly-Ser-cOHOrn, with a cyclicized portion present in two of the PVDs. For *P. fluorescens*, two of the PVDs had the same peptide chain of 13 amino acids, Ala-Lys-Gly-Gly-Ala-OHAsp-Gly-Ser-Ala-Ala-Ala-Ala-cOHOrn, whereas a third PVD had a Ser substituting for the first Ala. The side chain of the PVDs was either succinic acid or succinamide. The present approach can be employed for simultaneous structural characterization of several peptidic siderophores and related molecules in bacterial secretions.

Keywords Siderophore · Peptide · UHPLC · HR/AM

Introduction

Pseudomonas, a genus of aerobic gram-negative bacteria that are ubiquitous in natural soils and waters, are well known for their versatile adaptation to various environmental conditions [1–3]. In iron (Fe)-limited environments, the ability to produce siderophores confers a competitive advantage to fluorescent *Pseudomonas* (e.g., *P. putida*, *P. fluorescens*, *P. aeruginosa*, *P. syringae*, *P. chlororaphis*), which include plant-growth promoting bacteria as well as pathogenic bacteria [4]. Pyoverdine (PVD) is the primary high-affinity Fe-binding siderophore produced by fluorescent *Pseudomonas* [5–7]; other secreted siderophores have relatively lower affinity and produced in smaller quantity [5, 8, 9]. Therefore, of special interest is the characterization of the diverse PVD structures secreted by these *Pseudomonas* in an effort to obtain a comprehensive understanding of their Fe-transport mechanisms. The structures of PVDs have three common features: a 2,3-diamino-6,7-dihydroxyquinoline chromophore, a linear or cyclic peptide chain with 6 to 14 amino acids, and a side chain consisting of a dicarboxylic acid (succinic, α-ketoglutaric, glutamic, or malic acid) or its monoamide derivative [10]. The PVD structures have been considered potential

Electronic supplementary material The online version of this article (doi:10.1007/s00216-015-8659-5) contains supplementary material, which is available to authorized users.

✉ Ludmilla Aristilde
ludmilla@cornell.edu

[1] Department of Biological and Environmental Engineering, College of Agricultural and Life Sciences, Cornell University, Ithaca, NY 14853, USA

taxonomic markers to discriminate between different *Pseudomonas* strains [6, 11, 12]. From structures determined thus far, it appears that amino acid composition is strain-specific and that co-occurring PVDs only differ in the side chain identity [4, 10]. It is proposed that the PVD composition and geometry, particularly in the peptide backbone, mediate the recognition of the Fe-PVD complex by a specific membrane transporter [4]. Therefore, a high-resolution characterization of PVD structures is an important step toward elucidating the Fe-transport strategies employed by *Pseudomonas*.

A combination of electrophoretic characterization and cross uptake experiments with PVD-containing bacterial supernatants has been a common approach to type PVDs from different strains [10, 13]. However, PVDs with minor structural differences may have identical isoelectrophoretic patterns and Fe uptake behavior [10, 14]. Nuclear magnetic resonance (NMR) spectroscopy and tandem mass spectrometry (MS/MS) have become two important additional tools to characterize PVDs [10, 15–18]. NMR, however, typically requires sample purification for pre-isolation and high concentration of the target compounds. Tandem MS, which is commonly used in protein peptide sequencing [19–21], is an attractive technique for characterizing peptidic siderophores such as PVDs. The automated computational algorithms used in MS-based protein sequencing [20, 22, 23] are not ideal for PVD characterization due to the presence of a side chain, chromophore, and various modified and non-proteinogenic amino acids in the PVD structure [4]. However, manual characterization is feasible due to the moderate number of amino acids and the pre-knowledge of the chromophore in PVDs. Tandem MS has been applied in a few investigations of PVD structures [10, 15–18]. One study has used Fourier transform ion cyclotron resonance mass spectrometry (FTICR-MS) for high-resolution PVD structural determination [15]. However, a robust approach for the simultaneous determination of multiple PVD structures using high-resolution MS is largely lacking.

The ion trap-based collision-induced dissociation (CID) approach, which generates B and Y ions following cleavage of the peptide bond in a peptide chain [24, 25], has been applied in PVD structure characterization [10, 15–18] (Fig. 1). The doubly charged $[M+2H]^{2+}$ ion is typically used as a precursor for fragmentation due to its dominance over the singly charged $[M+H]^{+}$ ion. However, $[M+2H]^{2+}$ fragments often generate redundant and interfering ions that include doubly charged fragments, as well as ions resulting from the neutral loss of NH_3, H_2O, and CO from the B and Y ions [26, 27]. Interference by these fragments presents a challenge in PVD structural characterization, especially in low-resolution MS. The orbitrap-based higher-energy collisional dissociation (HCD) approach was shown to outperform CID by generating more fragments and providing more peptide identifications in proteomics [28–31]. Previous studies [32, 33] have reported an increased coverage of fragments for peptide sequencing when varied collision was applied. Stepped collision energies, which generate a variety of characteristic ions that are not often produced with a single collision energy, have also been shown to enhance characterization of small molecules [34]. Thus, combining differential collisional energies with high-resolution MS can facilitate the characterization of PVD structures.

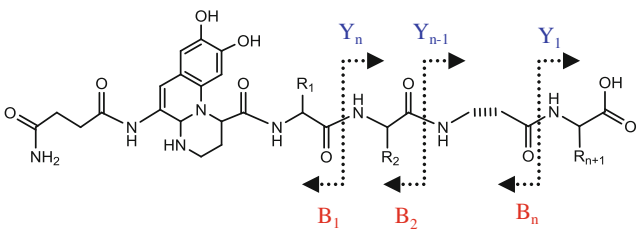

Fig. 1 Schematic illustration for the generation of B and Y ions from MS/MS fragmentation of PVDs

Here, we employed ultra-high performance liquid chromatography (UHPLC) and high-resolution/accurate-mass (HR/AM) quadrupole-orbitrap mass spectrometry to isolate, identify, and characterize multiple PVDs produced by two *Pseudomonas* strains (*Pseudomonas putida* KT2440 and *Pseudomonas fluorescens* RA12). The typical working resolution of the orbitrap mass analyzer can exceed 100,000 FWHM, which is comparable to that of FTICR-MS [35, 36]. The high-resolution offered by the orbitrap can resolve fragments with mass difference at ppm level that are irresolvable by low-resolution MS [37]. In addition, the high sensitivity of the orbitrap MS potentially allows the detection of a higher coverage of fragments to facilitate structure elucidation. Detection limits for small metabolites using orbitrap MS in the full scan mode were equivalent to or better than metabolite detection via triple quadrupole in the MS/MS mode [38]. Therefore, the coupling of UHPLC with the low detection and high-resolution capabilities of orbitrap MS provides an advantageous combination of instruments for our analytical approach.

In this study, we present a method for the characterization of PVDs in the extracellular matrix in the absence of any purification procedure. We applied varying HCD energies both to determine the optimal energy for the generation and to increase the coverage for the detection of B and Y ions. The measured masses of these ions were validated by matching with their theoretical exact masses. We were able to obtain the structure of multiple PVDs in the bacterial secretions with different side chains and/or peptide sequences. The approach described herein for multiple PVD structure characterization can be adopted to obtain the structures of peptidic siderophores and related quorum sensing molecules in bacterial secretions.

Materials and methods

Cultures and chemicals

P. putida (strain KT2440) was purchased from the American Type Culture Collection (ATCC; Manassas, VA). The soil isolate *P. fluorescens* (RA12) was a gift from Dr. Rania Abou-Kandil (Cornell University). The standard of pyoverdine produced by a *P. fluorescens* strain was purchased from Sigma-Aldrich (St. Louis, MO). Other chemicals (analytical grade) were purchased from Sigma-Aldrich (St. Louis, MO) or Fisher Scientific (Fair Lawn, NJ).

Growth conditions

Cell culturing was performed in 20-mL glass test tubes in a G24 environmental incubator shaker (New Brunswick Scientific, Edison, NJ) kept at 20 °C. The tubes were capped with sterilized sponge caps to avoid contamination from the air, while also allowing air circulation. The minimal growth medium included the following salts: 20 mM K_2HPO_4, 5 mM NaH_2PO_4, 0.8 mM $MgSO_4{\cdot}7H_2O$, 37 mM NH_4Cl, 34 μM $CaCl_2{\cdot}2H_2O$, 13 μM $CuSO_4{\cdot}5H_2O$, 0.49 μM H_3BO_3, 35 μM $ZnSO_4{\cdot}5H_2O$, 2.9 μM $MnSO_4{\cdot}5H_2O$, 0.11 μM $NiCl_2{\cdot}5H_2O$, and 0.6 μM $Na_2MoO_4{\cdot}5H_2O$. The minimal medium was pH-adjusted (pH 7.0) and filter-sterilized (0.22 μm). The cells were pre-cultured in Luria-Bertani liquid medium to saturation and subsequently transferred to the minimal medium in the absence (as a control) or in the presence of succinate (83.26 mM $Na_2C_4H_4O_4$) as a sole carbon source. The cells were grown under Fe-limiting condition where no exogenous Fe was added to the solution; background Fe was 37 nM measured via inductively coupled plasma atomic emission spectroscopy (ICP-AES, Spectro Analytical) analysis (detection limit=36 nM). Bacterial growth was monitored via optical density (OD_{600}), using an Agilent Cary 60 UV-visible spectrophotometer. All test tubes and vessels used for culturing and media storage were acid-washed and autoclaved before use.

Sample preparation

Bacterial samples (biological triplicates) were obtained at the onset of the stationary phase (~48 h) (see Electronic Supplementary Material Fig. S1). It was determined by fluorescence spectroscopy that the samples contained approximately 425 to 500 μM of total PVD concentration. Samples were centrifuged (15,000 rpm or 21,130*g*, 10 min) then filtered (0.22 μm nylon filters). The supernatants (10 μL injection volume) were then analyzed via LC-MS. To evaluate matrix effects on PVD isolation, the supernatants of *P. putida* (biological replicates) were subjected to a purification procedure adopted from a previous study [10]. Briefly, the pH-adjusted (pH 6) bacterial supernatants were passed through an Amberlite-XAD-4 column (20 cm length × 2.5 cm inner diameter). The column was first eluted with 100 mL MilliQ water and then 100 mL 1:1 water:methanol.

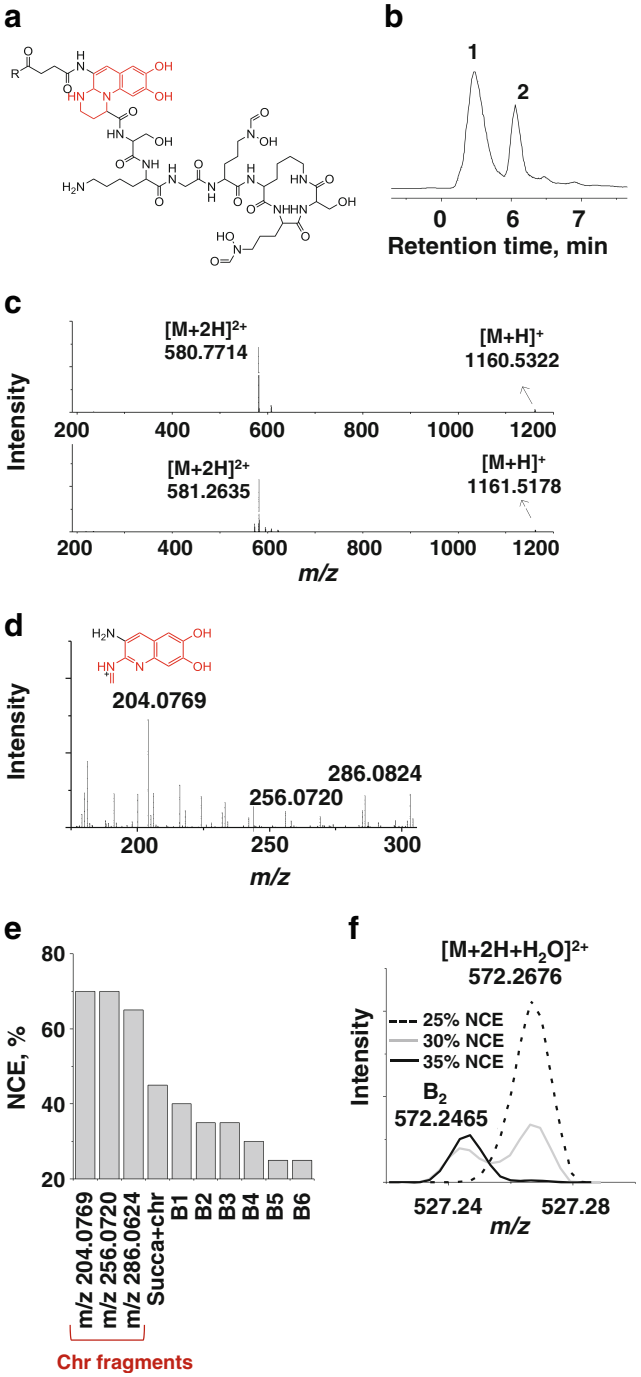

Fig. 2 Structural elucidation of pyoverdines in a standard solution. **a** Standard pyoverdine structures, R represents OH or NH_2. **b** MS full scan TIC. **c** ESI ions of the two major PVDs in the standard solution. **d** MS/MS fragments of chromophore obtained from $[M+2H]^{2+}$ at 40 % NCE. **e** Optimal NCEs required to cleave $[M+2H]^{2+}$ in standard PVD to generate listed fragments at the highest intensities. **f** Illustration of evolution of high-resolution MS/MS fragments at different NCEs

The PVDs were collected in the water/methanol fraction. The column was regenerated with 100 mL methanol/water followed by 100 mL water. The XAD-purified solutions were lyophilized and re-suspended in LC/MS-grade water.

All samples (both unpurified and purified supernatants) were diluted 1:5 with 50 mM acetic acid; the total PVD concentration in the analyte was about 85 to 100 μM. Examination of the total ion chromatograms (TIC) showed that chromatographic peaks in both samples were well resolved (Electronic Supplementary Material Fig. S2); details on how these peaks were obtained are detailed in the next section. Sequential sample injections showed that there was no noticeable signal suppression with the non-XAD-treated ones. Therefore, XAD treatment was not performed in order to avoid the loss of PVD amounts resulting from the XAD purification procedure. This allows more consistent results across replicates. As described in the following section, an ion fragmentation approach was implemented to facilitate the identification of PVD candidates from the non-purified bacterial secretions.

Characterization of PVDs

The characterization was conducted using a UHPLC (Thermo Scientific DionexUltiMate 3000 Rapid Separation LC) coupled with positive electrospray ionization (ESI) high-resolution accurate-mass (HR/AM) MS using the Thermo Scientific *Q Exactive* quadrupole-Orbitrap hybrid MS. The retention times of chromatographic peaks in the PVD-containing solutions were determined following passage through a Hypersil GOLD column (50×2.1 mm, 1.9 μm particle size, Thermo Scientific). The LC mobile phase consisted of a solution with 50 mM acetic acid (solvent A) and methanol (solvent B). The flow rate was 0.1 mL min^{-1}. A gradient separation procedure was used: solvent B was increased from 5 to 95 % within 15 min, 95 % solvent B was kept for 5 min, and then solvent B was returned to 5 % in 5 min before equilibrating the system at initial conditions for 5 min. The column temperature was 25 °C. Nitrogen gas (N_2) was used as sheath gas (flow rate of 30, arbitrary unit), auxiliary gas (12), and sweep gas (2). The spray voltage was 3.50 kV, capillary temperature was 230 °C, S-lens RF level was 55.0, and heater

Table 1 Theoretical and measured exact monoisotopic masses and compositions of B and Y ions generated by HCD fragmentation of $[M+2H]^{2+}$ of pyoverdines in the standard solution

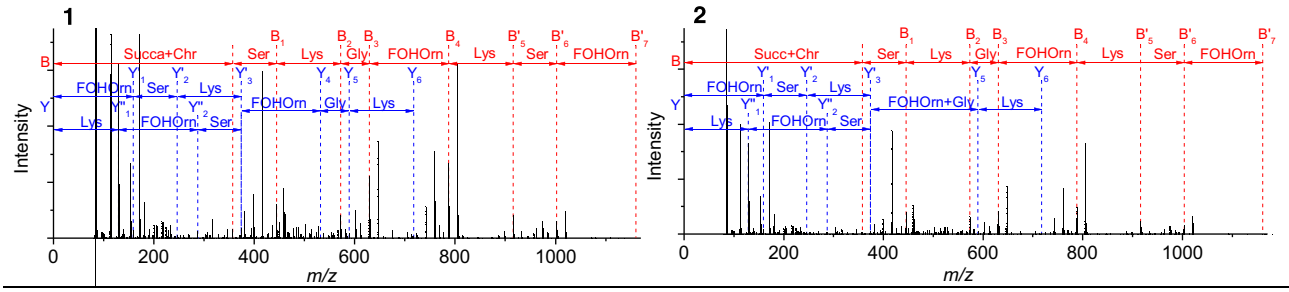

Fragment	Composition	Theoretical exact mass	Measured exact mass	δ_M ppm	Fragment	Composition	Theoretical exact mass	Measured exact mass	δ_M ppm
Succa +chr	$C_{17}H_{17}N_4O_5$	357.1199	357.1197	0.6	Succ +chr	$C_{17}H_{16}N_3O_6$	358.1039	358.1034	1.4
B_1	$C_{20}H_{22}N_5O_7$	444.1519	444.1517	0.5	B_1	$C_{20}H_{21}N_4O_8$	445.1359	445.1356	0.8
B_2	$C_{26}H_{34}N_7O_8$	572.2469	572.2465	0.7	B_2	$C_{26}H_{33}N_6O_9$	573.2309	573.2302	1.2
B_3	$C_{28}H_{37}N_8O_9$	629.2683	629.2673	1.7	B_3	$C_{28}H_{36}N_7O_{10}$	630.2524	630.2513	1.7
B_4	$C_{34}H_{47}N_{10}O_{12}$	787.3375	787.3360	1.9	B_4	$C_{34}H_{46}N_9O_{13}$	788.3215	788.3191	3.1
B'_5	$C_{40}H_{59}N_{12}O_{13}$	915.4325	915.4326	0.2	B'_5	$C_{40}H_{58}N_{11}O_{14}$	916.4165	916.4161	0.4
B'_6	$C_{43}H_{64}N_{13}O_{15}$	1002.4645	1002.4632	1.3	B'_6	$C_{43}H_{63}N_{12}O_{16}$	1003.4485	1003.4475	1.0
B'_7	$C_{49}H_{74}N_{15}O_{18}$	1160.5336	1160.5322	1.2	B'_7	$C_{49}H_{73}N_{14}O_{19}$	1161.5176	1161.5178	0.1
Y'_1	$C_6H_{11}N_2O_3$	159.0770	159.0766	2.3	Y'_1	$C_6H_{11}N_2O_3$	159.0770	159.0765	2.9
Y''_1	$C_6H_{13}N_2O$	129.1028	129.1024	3.0	Y''_1	$C_6H_{13}N_2O$	129.1028	129.1023	3.8
Y'_2	$C_9H_{16}N_3O_5$	246.1090	246.1085	2.0	Y'_2	$C_9H_{16}N_3O_5$	246.1090	246.1084	2.4
Y''_2	$C_{12}H_{23}N_4O_4$	287.1719	287.1717	0.8	Y''_2	$C_{12}H_{23}N_4O_4$	287.1719	287.1716	1.1
Y'_3	$C_{15}H_{28}N_5O_6$	374.2040	374.2037	0.7	Y'_3	$C_{15}H_{28}N_5O_6$	374.2040	374.2037	0.7
Y_4	$C_{21}H_{38}N_7O_9$	532.2731	532.2740	1.7	Y_4	$C_{23}H_{41}N_8O_{10}$	532.2731	--	
Y_5	$C_{23}H_{41}N_8O_{10}$	589.2946	589.2941	0.8	Y_5	$C_{23}H_{41}N_8O_{10}$	589.2946	589.2920	4.4
Y_6	$C_{29}H_{53}N_{10}O_{11}$	717.3895	717.3893	0.3	Y_6	$C_{29}H_{53}N_{10}O_{11}$	717.3895	717.3910	2.1

δ_M: mass accuracy (|theoretical mass - measured mass|/theoretical mass). *Succa* succinamide, *succ* succinic acid, *chr* chromophore, single or double prime: cyclic B or Y ions; – denotes not detectable

temperature was 300 °C. The *m/z* range was 190–1500. To ensure the *m/z* accuracy, the instrument was calibrated over the mass range of 195–1822 amu in the positive mode immediately prior to the analysis of the samples using the calibration solution provided by the manufacturer containing caffeine, the tetrapeptide MRFA (Met-Arg-Phe-Ala), and fluorinated phosphazines ultramark 1621. The external and internal mass deviations were within 0.3 ppm of the accurate masses of the calibration standards. The resolution was set to 70,000 in the full MS scan mode and all ion fragmentation (AIF) mode. The MS/MS spectra were acquired with 17,500 resolution.

As described above, in order to facilitate the application of our approach for PVD quantitation in addition to PVD characterization, the bacterial supernatants were not subjected to a purification step prior to the LC-MS analysis. To identify peaks of PVD candidates from the full scan TIC, the first step in our procedure was to extract fragmented ions of the 2,3-diamino-6, 7-dihydroxyquinoline chromophore from the TIC peaks of the bacterial secretions. We obtained characteristic ions of the chromophore through MS/MS fragmentation of the standard solution using the $[M+2H]^{2+}$ ion as a precursor. As collision-induced re-arrangement reactions have been observed for the doubly charged species [16], the singly charged molecular ion $[M+H]^{+}$ was also used as a precursor in the collision cell.

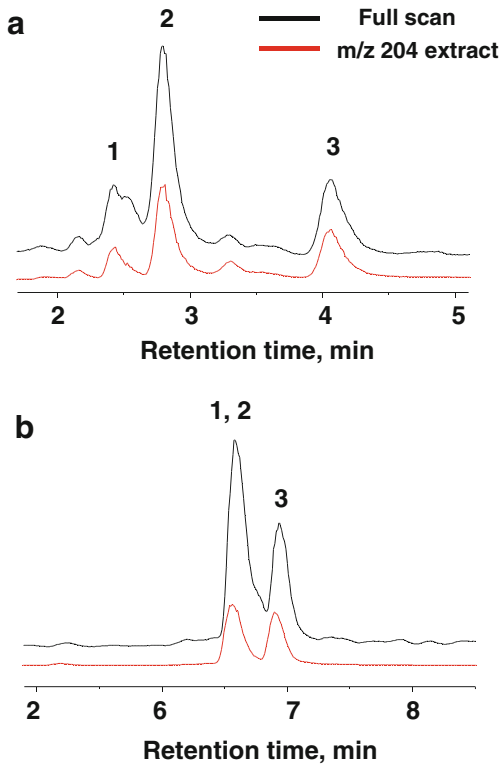

Fig. 3 MS full scan total ion chromatogram (*black*) and extracted ion chromatogram (extract: *m/z* 204.0773) of all ion fragmentation (*red*) obtained from extracellular media of *P. putida* (**a**) and *P. fluorescens* (**b**). Major PVD peaks were identified and numbered (also see Table 2)

Previous studies have shown that the CID fragments of PVD are enriched in B ions relative to Y ions [10, 16]. The chromophore ion (along with the side chain) was used as a starting point to define the B serial ions (Fig. 1). Varied collisional energies were used to generate the desired ions and increase the coverage of B and Y fragments as applied by previous studies on peptide sequencing [32, 33]. The collision cell energy was surveyed in the range of 20–70 % (with a 5 % increment) of the normalized collision energy (NCE). The different fragments as a function of the different collision energies exhibit different maximal intensities. By monitoring the changing trend of fragment intensities as a function of collision energies, we determined the required NCE for a maximum abundance of a B or Y ion, the collision energy window for adjacent B or Y

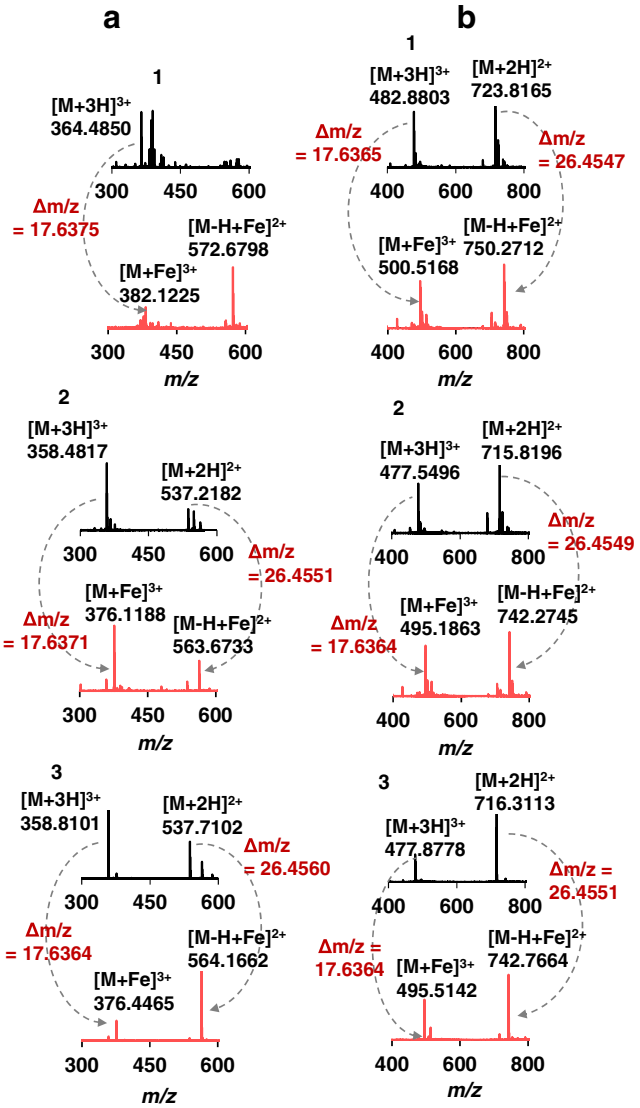

Fig. 4 ESI ions of the apo-PVDs (*black*) and Fe-complexed PVDs (*pink*) obtained with the extracellular matrix of *P. putida* (**a**, *left*) and *P. fluorescens* (**b**, *right*). The peptide sequence and the identity of the side chain moiety are tabulated in Table 2

fragments, and the resolution of subtle fragments that are only present around their optimal NCEs. This facilitated the determination of the identity of the different amino acid residues as well as their sequence in the PVD structure. The NCE was set to 50 % for the AIF mode. The selected B and Y ions in $[M+2H]^{2+}$ HCD process were confirmed with those in the $[M+H]^{+}$ fragmentation, whenever detectable.

We validated our approach by characterizing a solution with known PVD structures. Following method evaluation and validation with the standard solution, we applied our method to characterize PVDs in the bacterial samples. We note that the extraction step to identify PVD candidates was not necessary for the standard solution, which was a simple solution containing two known PVD structures.

Results and discussion

Method evaluation and validation

The two PVDs in the standard solution consist of the same peptide chain with the sequence Ser-Lys-Gly-FOHOrn-[Lys-Ser-FOHorn], and either succinamide or succinic acid as the side chain—FOHOrn is formyl hydroxyl-ornithine and the brackets indicate the cyclic portion of the peptide chain (Fig. 2a). Figure 2b illustrates the peaks for these two PVDs in the full scan TIC. In the positive ESI, each peak contained the $[M+2H]^{2+}$ ion as the major molecular ion and the $[M+H]^{+}$ as the minor ion (Fig. 2c). The detection limit for $[M+2H]^{2+}$ in the full MS scan mode was 10 ng/mL (or 8.6 nM). This low detection limit was also reported for orbitrap detection of small metabolites [34].

To characterize the PVD structures, the respective $[M+2H]^{2+}$ and $[M+H]^{+}$ ions were subjected to MS/MS fragmentation. We obtained three characteristic ions of the chromophore: *m/z* 204.0773 for the dihydroxyquinoline portion and *m/z* 256.0722 for the entire chromophore structure, *m/z* 286.0624 for the chromophore component connected to the dicarboxylic monoamide side chain [39] (Fig. 2d). The *m/z* 204.0773 ion, which is the most characteristic ion for the PVD chromophore following CID and HCD [10, 39], was the most abundant at 40 % NCE (Fig. 2d). We monitored the trend of fragment intensities as a function of collision energies. Our results indicate that the HCD fragmentation of PVDs occurred in a stepwise manner whereby the intensity of ions was dependent on the collision energy applied (Fig. 2e). Figure 2e shows the optimal NCEs for obtaining the different targeted MS/MS fragments of the standard PVD structure at maximum intensity. We determined that the NCE necessary for detecting a maximum abundance of a B or Y ion was between the NCEs of its immediate precursor and product (Fig. 2e). Furthermore, the different NCEs can be useful in identifying interfering ions. For instance, $[C_{49}H_{74}N_{15}O_{18}+2H-H_2O]^{2+}$ could interfere with the detection of the B2 fragment $[C_{26}H_{34}N_7O_8]^{+}$ in low-resolution MS. In the orbitrap MS, we distinguished between these two fragments by adjusting the NCE applied for the fragmentation (Fig. 2f). We were able to resolve B2 from the doubly charged species by targeting B2 at 30 % NCE or higher (Fig. 2f). Our results thus demonstrate that the application of a single collision energy or a small window of collision energy is limiting in the ability to capture a high coverage of MS/MS fragments of PVD as well as detecting interfering ions. Our method thus overcomes this limitation.

The exact monoisotopic mass of the chromophore with the side chain was 357.1199 (with the succinic acid as the side chain) and 358.1039 (with succinamide as the side chain) (Table 1). These two ions served as the starting point to define the B serial ions (Table 1). The starting point for the Y ion series was based on the a priori knowledge that PVD biosynthesis is initiated from the formation of hydroxyornithine (OHOrn) [6], which is commonly detected at the terminal end, either as FOHOrn or cyclo-hydroxyornithine (cOHOrn), of the majority of PVDs produced by *Pseudomonas* [4, 10]. The detection of *m/z*

Table 2 Structural characterization of major PVDs secreted by the two *Pseudomonas* strains

PVD#	RT	$[M+2H]^{2+}$	$[M+H]^{+}$	Identity of side chain and peptide sequence
P. putida KT2440				
1	2.47	546.2232	1091.4395	**succa**-chr-Asp-Orn-**OHAsp-Dab**-Gly-Ser-cOHOrn
2	2.75	537.2177	1073.4284	**succa**-chr-Asp-Orn-[**OHAsp-Dab**]-Gly-Ser-cOHOrn
3	3.93	537.7099	1074.4123	**succ**-chr-Asp-Orn-[**OHAsp-Dab**]-Gly-Ser-cOHOrn
P. fluorescens RA12				
1	6.60	723.8135	1446.6206	**succa**-chr-**Ser**-Lys-Gly-Gly-Ala-OHAsp-Gly-Ser-Ala-Ala-Ala-Ala-cOHOrn
2	6.62	715.8180	1430.6300	**succa**-chr-**Ala**-Lys-Gly-Gly-Ala-OHAsp-Gly-Ser-Ala-Ala-Ala-Ala-cOHOrn
3	6.93	716.3095	1431.6124	**succ**-chr-**Ala**-Lys-Gly-Gly-Ala-OHAsp-Gly-Ser-Ala-Ala-Ala-Ala-cOHOrn

RT retention time (min). $[M+H]^{+}$ and $[M+2H]^{2+}$ singly and doubly monoisotopic molecular ions. Brackets indicate a cyclic structure. Succ represents succinic acid and succa represents succinamide. Unusual or modified amino acids: OHAsp (hydroxyaspartic acid), Dab (diaminobutanoic acid), cOHOrn (cyclo-hydroxyornithine). The parts that are different in the PVD structures produced by each strain are shown in bold

159.0770 in the standard solution was assigned to the presence of FOHOrn.

The initial assignments of the first B and Y ions in the series facilitated the identification of subsequent B and Y ions in the PVD structure (Table 1). The MS/MS spectra generated at 35 % NCE using the $[M+2H]^{2+}$ ion of the two PVDs and the resulting B and Y ions are shown in Table 1. Table 1 shows the comparisons of the theoretical and measured exact masses of the identified B and Y ions, which illustrate our ability to achieve high mass accuracy detection of these ions, within 4.4 ppm or lower. We detected two series of Y ions and the full series of B ions (Table 1). From the two Y serial ions, we resolved that the linear structure of the PVD from the chromophore end is up to FOHOrn attached to Lys, which combines with Ser and FOHorn to form the cyclic portion in the peptide chain. In a previous study, using low-resolution quadrupole-ion trap MS, an additional CID fragmentation was performed in order to determine the arrangement of the tripeptide cycle in the same PVD [15]. Our findings demonstrate that we were able to determine the cyclic portion with the high-resolution and sensitive detection of the MS/MS HCD fragmentation approach (Table 1).

The co-existing pair of PVD structures in the standard solution, which differs only in the side chain, is typical [4]. Both structures share the same Y serial ions, but differ by 0.9840 Da in their $[M+H]^+$, singly charged B ions and associated ions from neutral losses, and 0.4920 Da in their doubly charged counterparts (Table 1). A simultaneous structural characterization was applied because the two PVDs share a similar fragmentation pattern (Table 1). And, we were able to distinguish the presence of the different side chains by monitoring the *m*/*z* difference (Table 1).

Identification of PVDs in the bacterial samples

The full TIC spectra of the bacterial supernatants of each strain are illustrated in Fig. 3. Multiple peaks were present consisting of singly charged ions in the range of 800–1500 Da. The molecular ions of the compounds were found in singly ($[M+H]^+$), doubly ($[M+2H]^{2+}$), and triply ($[M+3H]^{3+}$) charged forms, with the former two being more abundant. Each bacterial sample was analyzed in AIF mode at 50 % NCE, in order to generate the peak of the chromophore fragment at *m*/*z* 204.0773 with a decent intensity. This fragment ion was used for screening the full scan TIC peaks for PVD candidates (Fig. 3). We determined that there were three major PVD candidates in the *P. putida* supernatant and three in the *P. fluorescens* supernatant (Fig. 3a, b, respectively). The singly and doubly charged ions of these PVD candidates were used for subsequent MS/MS structure characterization.

In order to confirm that the identified PVDs can indeed complex Fe, we reacted our bacterial supernatants with an excess of Fe^{3+}. The TIC spectra illustrated the disappearance of the peaks of the free PVDs following Fe-complexation (Electronic Supplementary Material Fig. S3). Instead, the Fe-complexed PVDs were detected as earlier eluants (Electronic

Table 3 Theoretical and measured exact monoisotopic masses and compositions of B and Y ions generated via HCD fragmentation

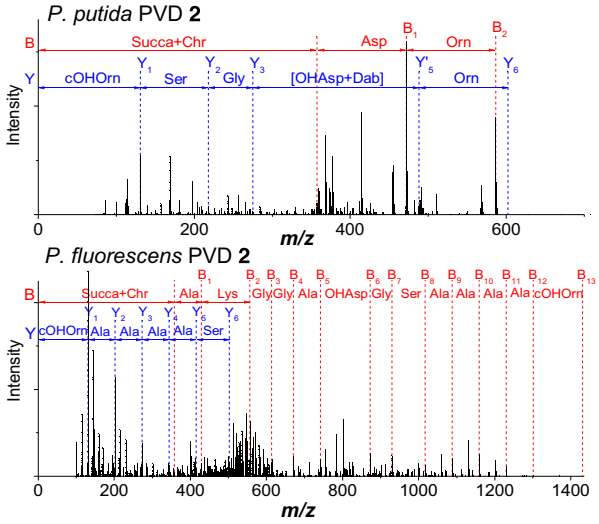

Fragment	Composition	Theoretical exact mass	Measured exact mass	δ_M ppm
P. putida PVD **2**				
Succa+chr	$C_{17}H_{17}N_4O_5$	357.1199	357.1199	0
B_1	$C_{21}H_{22}N_5O_8$	472.1468	472.1468	0.1
B_2	$C_{26}H_{32}N_7O_9$	586.2262	586.2258	0.6
Y_1	$C_5H_{11}N_2O_2$	131.0821	131.0817	2.7
Y_2	$C_8H_{16}N_3O_4$	218.1141	218.1139	0.8
Y_3	$C_{10}H_{19}N_4O_5$	275.1355	275.1351	1.6
Y'_5	$C_{18}H_{30}N_7O_9$	488.2105	488.2104	0.2
Y_6	$C_{23}H_{40}N_9O_{10}$	602.2898	602.2896	0.4
P. fluorescens PVD **2**				
Succa+chr	$C_{17}H_{17}N_4O_5$	357.1199	357.1199	0
B_1	$C_{20}H_{22}N_5O_6$	428.1570	428.1570	0
B_2	$C_{26}H_{34}N_7O_7$	556.2520	556.2520	0.1
B_3	$C_{28}H_{37}N_8O_8$	613.2734	613.2731	0.5
B_4	$C_{30}H_{40}N_9O_9$	670.2949	670.2950	0.2
B_5	$C_{33}H_{45}N_{10}O_{10}$	741.3320	741.3340	2.7
B_6	$C_{37}H_{50}N_{11}O_{14}$	872.3539	872.3536	0.3
B_7	$C_{39}H_{53}N_{12}O_{15}$	929.3753	929.3743	1.1
B_8	$C_{42}H_{58}N_{13}O_{17}$	1016.4074	1016.4080	0.6
B_9	$C_{45}H_{63}N_{14}O_{18}$	1087.4445	1087.4456	1.0
B_{10}	$C_{48}H_{68}N_{15}O_{19}$	1158.4816	1158.4811	0.4
B_{11}	$C_{51}H_{73}N_{16}O_{20}$	1229.5187	1229.5168	1.5
B_{12}	$C_{54}H_{78}N_{17}O_{21}$	1300.5558	1300.5531	2.1
B_{13}	$C_{59}H_{88}N_{19}O_{23}$	1430.6300	1430.6286	1.0
Y_1	$C_5H_{11}N_2O_2$	131.0821	131.0817	2.7
Y_2	$C_8H_{16}N_3O_3$	202.1192	202.1190	0.8
Y_3	$C_{11}H_{21}N_4O_4$	273.1563	273.1560	1.0
Y_4	$C_{14}H_{26}N_5O_5$	344.1934	344.1933	0.3
Y_5	$C_{17}H_{31}N_6O_6$	415.2305	415.2301	1.0
Y_6	$C_{20}H_{36}N_7O_8$	502.2625	502.2625	0.1

δ_M: mass accuracy (|theoretical mass - measured mass|/theoretical mass).
Succa succinamide, *succ* succinic acid, *chr* chromophore

Supplementary Material Fig. S3). The relative abundances of the complexes were similar to those of the free PVDs (Electronic Supplementary Material Fig. S3). We obtained triply ($[M+Fe]^{3+}$), doubly ($[M-H+Fe]^{2+}$), and singly ($[M-2H+Fe]^{+}$) charged ions of the PVD-Fe complexes were present, with the former two being in a higher abundance (Fig. 4).

Structural characterization of PVDs in bacterial samples

Using the same approach detailed in the "Method evaluation and validation" section, we characterized the structures of the three PVDs in the *P. putida* and *P. fluorescence* supernatant solutions (Tables 2 and 3 and Fig. 5). The starting B ion for the B series was analogous to what was determined for the standard solution, thus indicating that the PVDs in our samples has either succinic acid or succinamide as the side chain. However, the starting Y serial ion was different. The detection of *m/z* 131.0821 was assigned to the presence of cyclo-hydroxyornithine (cOHOrn). All the PVDs possess OHAsp within the peptide chain, cOHOrn (at one end of peptide chain), in addition to the dihydroquinoline chromophore (at the other end); these moieties have been proposed as the ligand sites for the complexation of Fe [40] (Table 2 and Fig. 5.). The MS/MS spectra and the detected B and Y ions of the most abundant PVD from each strain (PVD **2** from *P. putida* and PVD **2** from *P. fluorescens*) are shown in Table 3. For the *P. putida* PVD **2**, only the smaller B and Y ions were detected; for the *P. fluorescens* PVD **2**, all B ions were obtained, whereas only the initial Y ions were detected (Table 3). These ions were obtained from the MS/MS fragments of $[M+2H]^{2+}$ at 35 and 30 % NCE for *P. putida* and *P. fluorescens*, respectively. The comparison of the theoretical and measured exact masses of the identified B and Y ions, shown in Table 3, illustrates our ability to detect these ions with high mass accuracy (within 2.7 ppm or less).

The full structure derived for *P. putida* PVD **2** (Table 2 and Fig. 5a), which consists of seven amino acids, is in partial agreement with the predicted peptide chain of OHAsp-Lys-OHAsp-Dab-Gly-Ser-Orn based on silico analysis of non-ribosomal peptide synthetases genes [41], but is identical to the structure determined via isoelectrofocusing method [9] and via fast atom bombardment MS coupled with NMR [42]. Two additional PVD structures (**1** and **3**) were characterized in the secretion of the *P. putida* strain (Table 2 and Fig. 5). The cyclicized OHAsp-Dab in PVD **2** and PVD **3** was linear in PVD **1** (Table 2 and Fig. 5a). Both structural arrangements (cyclic and linear) have been reported among the different

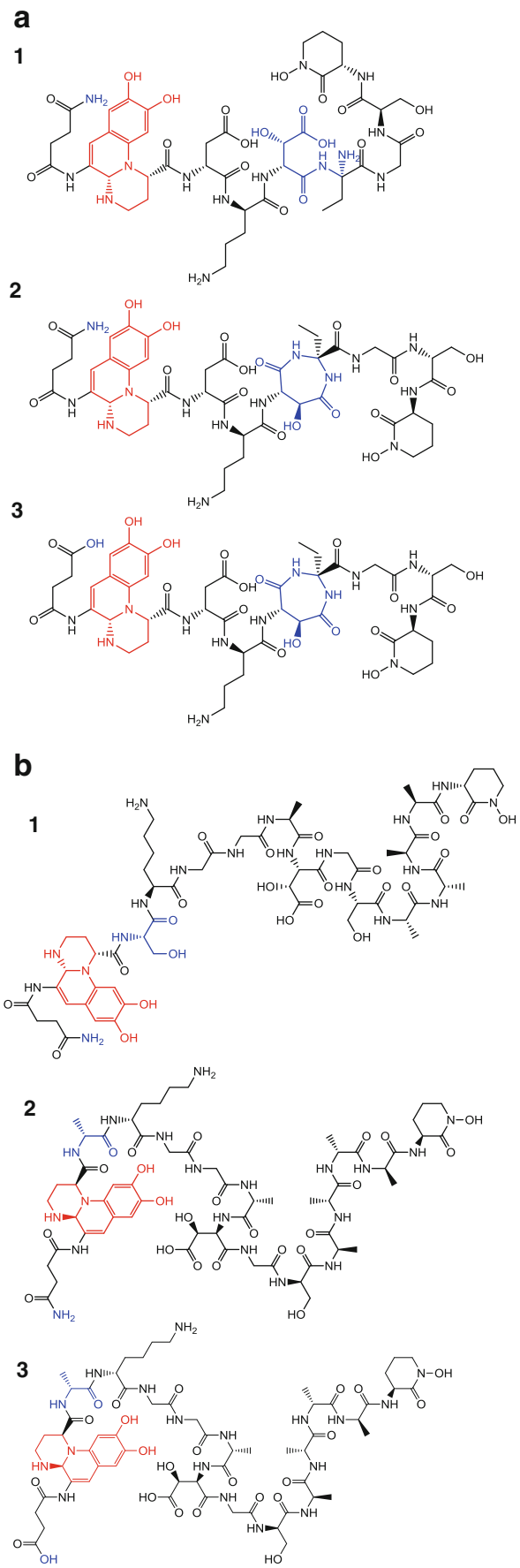

Fig. 5 Chemical structures of the three major PVDs characterized in the bacterial secretion of *P. putida* (**a**) and *P. fluorescens* (**b**). The chromophore is shown in *red* and the moieties that are different among the structures are shown in *blue*. Structures were drawn using ChemDraw Pro.Version 14.0.0.117

PVDs produced by *Pseudomonas* strains [4]. Our high-resolution MS analysis thus provides evidence that both arrangements of the peptide chain can exist in the extracellular medium of one strain. PVDs **2** and **3** have the same linear peptide sequence and differ only in the side chain (succinic amide and succinic acid, respectively) (Table 2 and Fig. 5).

With respect to the three major PVD produced by *P. fluorescens*, we determined that all three have a linear peptide chain consisting of a sequence of 13 amino acid residues (Table 2 and Fig. 5b). The peptide sequence of PVD **2** closely resembles that of another previously reported PVD sequence, Ala-Lys-Gly-Gly-OHAsp-Gln-Ser-Ala-Ala-Ala-Ala-cOHOrn, from *P. fluorescens* with a molecular mass of 1430 [43]; the only difference between the two structures is that one of the Gly residues in the PVD **2** is replaced by a Gln in the reported PVD. Similar to *P. putida* PVDs **2** and **3**, *P. fluorescens* PVDs **2** and **3** only differ in the side chain whereby the former has a succinamide, whereas the latter has a succinic acid (Table 2). Compared with PVD **2**, PVD **1** produced by *P. fluorescens* has a Ser substituting for the Ala as the first amino acid residue attached to the chromophore (Table 2), thus indicating that the same strain may produce PVDs with a different peptide sequence.

Conclusions

Pseudomonas and related bacteria secrete peptidic siderophores in response to Fe-limited nutritional environments. A simple and fast approach for obtaining high-resolution characterization of these molecules in bacterial secretions is an important step toward elucidating the Fe-transport mechanisms of these bacteria. In addition to avoiding analyte losses, the absence of purification steps in the presented method simplified and sped up the characterization procedure. The combination of LC with quadrupole-orbitrap MS along with the application of multiple HCD energies can be applied to facilitate, with high-resolution and high-mass accuracy, the structural elucidation of multiple peptidic siderophores in a bacterial secretion.

Acknowledgments We are grateful to Dr. Rania Abou-Kandil for providing the *P. fluorescens* strain. We thank David F. Flannelly and Matthew A. Kukurugya for commenting on earlier versions of the manuscript. This work was supported in part by a Research Starter grant from the U.S. National Science Foundation (SSB 1337292) from the Division of Systems and Synthetic Biology.

References

1. Poblete-Castro I, Becker J, Dohnt K, dos Santos V, Wittmann C (2012) Industrial biotechnology of Pseudomonas putida and related species. Appl Microbiol Biotechnol 93(6):2279–2290
2. Spiers AJ, Buckling A, Rainey PB (2000) The causes of Pseudomonas diversity. Microbiology 146(10):2345–2350
3. Silby MW, Winstanley C, Godfrey SAC, Levy SB, Jackson RW (2011) Pseudomonas genomes: diverse and adaptable. FEMS Microbiol Rev 35(4):652–680
4. Cezard C, Farvacques N, Sonnet P (2015) Chemistry and biology of Pyoverdines, pseudomonas primary siderophores. Curr Med Chem 22(2):165–186
5. Cornelis P, Matthijs S (2007) Pseudomonas siderophores and their biological significance. In: Varma A, Chincholkar S (eds) Microbial siderophores, vol 12. Soil biology. Springer, Berlin, pp 193–203
6. Meyer J-M (2000) Pyoverdines: pigments, siderophores and potential taxonomic markers of fluorescent Pseudomonas species. Arch Microbiol 174(3):135–142
7. Visca P, Imperi F, Lamont IL (2007) Pyoverdine siderophores: from biogenesis to biosignificance. Trends Microbiol 15(1):22–30
8. Cornelis P (2010) Iron uptake and metabolism in pseudomonads. Appl Microbiol Biotechnol 86(6):1637–1645
9. Matthijs S, Laus G, Meyer J-M, Abbaspour-Tehrani K, Schäfer M, Budzikiewicz H, Cornelis P (2009) Siderophore-mediated iron acquisition in the entomopathogenic bacterium Pseudomonas entomophila L48 and its close relative Pseudomonas putida KT2440. BioMetals 22(6):951–964
10. Meyer J-M, Gruffaz C, Raharinosy V, Bezverbnaya I, Schäfer M, Budzikiewicz H (2008) Siderotyping of fluorescent Pseudomonas: molecular mass determination by mass spectrometry as a powerful pyoverdine siderotyping method. BioMetals 21(3):259–271
11. Meyer J-M, Geoffroy VA, Baida N, Gardan L, Izard D, Lemanceau P, Achouak W, Palleroni NJ (2002) Siderophore typing, a powerful tool for the identification of fluorescent and nonfluorescent pseudomonads. Appl Environ Microbiol 68(6):2745–2753
12. Meyer J-M (2010) Pyoverdine siderophores as taxonomic and phylogenic markers. In: Ramos JL, Filloux A (eds) Pseudomonas. Springer, Netherlands, pp 201–233
13. Meyer J-M, Stintzi A, Coulanges V, Shivaji S, Voss JA, Taraz K, Budzikiewic H (1998) Siderotyping of fluorescent pseudomonads: characterization of pyoverdines of Pseudomonas fluorescens and Pseudomonas putida strains from Antarctica. Microbiology 144(11):3119–3126
14. Bultreys A, Gheysen I, Wathelet B, Maraite H, de Hoffmann E (2003) High-performance liquid chromatography analyses of pyoverdin siderophores differentiate among phytopathogenic fluorescent Pseudomonas species. Appl Environ Microbiol 69(2):1143–1153
15. Schäfer M, Fuchs R, Budzikiewicz H, Springer A, Meyer J-M, Linscheid M (2006) Structure elucidation of cyclic pyoverdins and examination of rearrangement reactions in MS/MS experiments by determination of exact product ion masses. J Mass Spectrom 41(9):1162–1170
16. Fuchs R, Budzikiewicz H (2001) Rearrangement reactions in the electrospray ionization mass spectra of pyoverdins. Int J Mass Spectrom 210–211:603–612
17. Fuchs R, Budzikiewicz H (2001) Structural studies of pyoverdins by mass spectrometry. Curr Org Chem 5(3):265–288
18. Budzikiewicz H, Schafer M, Fernandez DU, Meyer J (2006) Structure proposal for a new pyoverdin from Pseudomonas sp. PS 6.10. Z Naturforsch C 61(11/12):815
19. Domon B, Aebersold R (2006) Mass spectrometry and protein analysis. Science 312(5771):212–217
20. Aebersold R, Mann M (2003) Mass spectrometry-based proteomics. Nature 422(6928):198–207
21. Aebersold R, Goodlett DR (2001) Mass spectrometry in proteomics. Chem Rev 101(2):269–296
22. Eng J, McCormack A, Yates J (1994) An approach to correlate tandem mass spectral data of peptides with amino acid sequences in a protein database. J Am Soc Mass Spectrom 5(11):976–989

23. Perkins DN, Pappin DJC, Creasy DM, Cottrell JS (1999) Probability-based protein identification by searching sequence databases using mass spectrometry data. Electrophoresis 20(18): 3551–3567
24. Steen H, Mann M (2004) The abc's (and xyz's) of peptide sequencing. Nat Rev Mol Cell Biol 5(9):699–711
25. Roepstorff P, Fohlman J (1984) Proposal for a nomenclature for sequence ions in mass spectra of peptides. Biomed Mass Spectrosc 11:601
26. Dongré AR, Jones JL, Somogyi Á, Wysocki VH (1996) Influence of peptide composition, gas-phase basicity, and chemical modification on fragmentation efficiency: evidence for the mobile proton model. J Am Chem Soc 118(35):8365–8374
27. Tang XJ, Thibault P, Boyd RK (1993) Fragmentation reactions of multiply-protonated peptides and implications for sequencing by tandem mass spectrometry with low-energy collision-induced dissociation. Anal Chem 65(20):2824–2834
28. Nilsson CL (2011) Advances in quantitative phosphoproteomics. Anal Chem 84(2):735–746
29. Jedrychowski MP, Huttlin EL, Haas W, Sowa ME, Rad R, Gygi SP (2011) Evaluation of HCD- and CID-type fragmentation within their respective detection platforms for murine phosphoproteomics. Mol Cell Proteomics 10(12):M111.009910
30. Frese CK, Altelaar AFM, Hennrich ML, Nolting D, Zeller M, Griep-Raming J, Heck AJR, Mohammed S (2011) Improved peptide identification by targeted fragmentation using CID, HCD and ETD on an LTQ-Orbitrap Velos. J Proteome Res 10(5):2377–2388
31. Shen Y, Tolić N, Xie F, Zhao R, Purvine SO, Schepmoes AA, Moore RJ, Anderson GA, Smith RD (2011) Effectiveness of CID, HCD, and ETD with FT MS/MS for degradomic-peptidomic analysis: comparison of peptide identification methods. J Proteome Res 10(9):3929–3943
32. Diedrich J, Pinto AM, Yates J III (2013) Energy dependence of HCD on peptide fragmentation: stepped collisional energy finds the sweet spot. J Am Soc Mass Spectrom 24(11):1690–1699
33. Neta P, Simon-Manso Y, Yang X, Stein SE (2009) Collisional energy dependence of peptide ion fragmentation. J Am Soc Mass Spectrom 20(3):469–476
34. Bushee JL, Argikar UA (2011) An experimental approach to enhance precursor ion fragmentation for metabolite identification studies: application of dual collision cells in an orbital trap. Rapid Commun Mass Spectrom 25(10):1356–1362
35. Scigelova M, Makarov A (2006) Orbitrap mass analyzer—overview and applications in proteomics. Proteomics 6(S2):16–21
36. Denisov E, Damoc E, Lange O, Makarov A (2012) Orbitrap mass spectrometry with resolving powers above 1,000,000. Int J Mass Spectrom 325–327:80–85
37. Zhang Y, Hao Z, Kellmann M, Huhmer A (2012) HR/AM targeted peptide quantitation on a Q Exactive MS: a unique combination of high selectivity, sensitivity and throughput. SRM 6:7
38. Lu W, Clasquin MF, Melamud E, Amador-Noguez D, Caudy AA, Rabinowitz JD (2010) Metabolomic analysis via reversed-phase ion-pairing liquid chromatography coupled to a stand alone Orbitrap Mass Spectrometer. Anal Chem 82(8):3212–3221
39. Budzikiewicz H, Schäfer M, Fernández D, Matthijs S, Cornelis P (2007) Characterization of the chromophores of pyoverdins and related siderophores by electrospray tandem mass spectrometry. BioMetals 20(2):135–144
40. Hider RC, Kong X (2010) Chemistry and biology of siderophores. Nat Prod Rep 27(5):637–657
41. Ravel J, Cornelis P (2003) Genomics of pyoverdine-mediated iron uptake in pseudomonads. Trends Microbiol 11(5):195–200
42. Salah El Din ALM, Kyslík P, Stephan D, Abdallah MA (1997) Bacterial iron transport: structure elucidation by FAB-MS and by 2D NMR (1H, 13C, 15N) of pyoverdin G4R, a peptidic siderophore produced by a nitrogen-fixing strain of Pseudomonas putida. Tetrahedron 53(37):12539–12552
43. Mohn G, Taraz K, Budzikiewicz H, Naturforsch Z (1990) New pyoverdin-type siderophores from Pseudomonas fluorescens. Z Naturforsc B J Chem Sci 45(10):1437–1450